A link between the hiatus in global warming and North American drought

Thomas L. Delworth[1], Fanrong Zeng[1], Anthony Rosati[1,2], Gabriel Vecchi[1], and Andrew Wittenberg[1]

[1]Geophysical Fluid Dynamics Laboratory/NOAA

201 Forrestal Rd.

Princeton, NJ 08540 USA

[2]University Corporation for Atmospheric Research (UCAR)

Revised version submitted to *Journal of Climate*

February 19, 2015

Corresponding author: Thomas L. Delworth

E-Mail: tom.delworth@noaa.gov
Phone: 609-452-6565

Postal:
Geophysical Fluid Dynamics Laboratory/NOAA
201 Forrestal Rd.
Princeton University Forrestal Campus
Plainsboro, NJ 08540
USA

Abstract

Portions of western North America have experienced prolonged drought over the last decade. This drought has occurred at the same time as the global warming hiatus – a decadal period with little increase in global mean surface temperature. We use climate models and observational analyses to clarify the dual role of recent tropical Pacific changes in driving both the global warming hiatus and North American drought. When we insert observed tropical Pacific wind stress anomalies into coupled models, the simulations produce persistent negative sea surface temperature anomalies in the eastern tropical Pacific, a hiatus in global warming, and drought over North America driven by SST-induced atmospheric circulation anomalies. In our simulations the tropical wind anomalies account for 92% of the simulated North American drought during the recent decade, with 8% from anthropogenic radiative forcing changes. This suggests that anthropogenic radiative forcing is not the dominant driver of the current drought, unless the wind changes themselves are driven by anthropogenic radiative forcing. The anomalous tropical winds could also originate from coupled interactions in the tropical Pacific or from forcing outside the tropical Pacific. The model experiments suggest that if the tropical winds were to return to climatological conditions, then the recent tendency toward North American drought would diminish. Alternatively, if the tropical winds were to persist, then the impact on North American drought would continue; however, the impact of the enhanced Pacific easterlies on global temperature diminishes after a decade or two due to a surface reemergence of warmer water that was initially subducted into the ocean interior.

1. Introduction

There has been a prolonged drought over portions of western North America since around the year 2000 (Stahle et al. 2009; Cayan et al. 2010; Seager and Hoerling 2014), encompassing regions from the western Plains to the West Coast. This decadal-scale drought has created substantial impacts in many societal sectors, including agriculture and wildfires (Dennison et al. 2014). The underlying causes of the drought are not well established in terms of the role of natural variability versus human-induced radiative forcing changes, such as from increasing greenhouse gases. Recent work focusing on California drought during the shorter 2011-2014 period has suggested that internal variability is likely responsible (Wang and Schubert 2014a; Funk et al. 2014; Seager et al. 2015), although aspects of the atmospheric circulation associated with that drought could have some relationship to climate change (Swain et al. 2014). The causes of the larger-scale decadal drought over western North America are less clear. This decadal-scale drought has occurred at the same time as the so-called global warming hiatus(Easterling and Wehner 2009; Bindoff, N.L., et al. 2013; Hawkins et al. 2014), a decadal period with little increase in global mean surface temperature. In this study we find a clear link between the hiatus and recent decadal-scale drought over portions of North America via enhanced easterly winds in the tropical Pacific and their association with decadal changes in local sea-surface temperature.

There are a number of factors that could have contributed to the recent observed hiatus in global warming (Clement and DiNezio 2014), including natural radiative forcing, anthropogenic radiative forcing, and internal variability of the climate system. Potential natural radiative forcing factors include volcanic activity (Santer et al. 2014) and a persistently low level of solar irradiance in the most recent solar cycle, in addition to changes in stratospheric water vapor(Solomon et al. 2010). An

altered vertical distribution of heating within the ocean could have also contributed to the hiatus (Trenberth and Fasullo 2013; Katsman and van Oldenborgh 2011; Balmaseda et al. 2013). The hiatus could also have substantial contributions from internal variability of the coupled system, linked to phenomena such as ENSO and the Pacific Decadal Oscillation(Meehl et al. 2011, 2013; Vecchi and Wittenberg 2010; Ogata et al. 2013) or the Atlantic Multidecadal Oscillation(Tung and Zhou 2013). It has also been suggested that incomplete coverage in observing systems(Cowtan and Way 2014) could have led to underestimation of the true warming trend.

Recent work has highlighted the importance of observed changes in the tropical Pacific for explaining the hiatus in global warming. Kosaka and Xie (2013) were able to simulate the hiatus using a global climate model when sea surface temperatures (SSTs) over the eastern near-equatorial Pacific were strongly damped towards observed SSTs. England et al. (2014) extended this work by first noting that the hiatus period has exhibited unusually intense easterly winds in the tropical Pacific. They then showed that these enhanced easterly winds in the Pacific lead a climate model to replicate many aspects of the observed hiatus, including global mean surface air temperature and the patterns of upper ocean heat content change. Taken together, Kosaka and Xie (2013) and England et al. (2014) indicate that much of the hiatus may be connected to tropical Pacific SST and wind stress changes. Recent work has suggested that the enhanced tropical Pacific easterly winds could be partly driven from regions outside the Pacific, whether from the Indian Ocean (Luo et al. 2012) or the Atlantic (McGregor et al. 2014).

In the current study we use numerical modeling experiments to explore the relationships between enhanced tropical Pacific easterly winds and global climate. The results of our experiments, done with

a suite of different models, independently confirm the results of England et al (2014) and support the conclusions of Kosaka and Xie (2013). Further, we show a strong connection between these same tropical Pacific wind stress changes and drought over North America. Our results suggest that the observed drought over portions of western North America over the last decade is not likely to be a direct response of the climate system to radiative forcing changes, unless the wind stress changes themselves are induced by radiative forcing changes. We also show, using idealized experiments, that the impact of constant easterly tropical Pacific wind anomalies on simulated global-mean temperature appears to be transient, diminishing after a decade or two.

2. Model, simulations, and observational data

a. Model and simulations

We use targeted numerical experiments with multiple comprehensive climate models in concert with observational analyses. We use three models: (a) the Geophysical Fluid Dynamics Laboratory (GFDL) CM2.1 model(Delworth et al. 2006; Wittenberg et al. 2006); (b) the GFDL CM2.5_FLOR model (Vecchi et al. 2014), hereafter referred to as "FLOR"; and (c) the GFDL CM2.5_FLOR_FA model (Vecchi et al. 2014), hereafter referred to as FLOR_FA. All three models share many aspects of their physics, and have very similar ocean models, but differ in atmospheric resolution. The CM2.1 model has an atmospheric horizontal grid-spacing of ~200 Km, with 24 vertical levels. The FLOR and FLOR_FA models derive from the GFDL CM2.5 model (Delworth et al. 2012), and have atmospheric grid-spacing of ~50 Km in the horizontal, with 32 levels in the vertical, and a more sophisticated land model than the CM2.1 model. The FLOR_FA model differs from FLOR through the use of flux adjustments (Magnusson et al. 2013) as a numerical technique to reduce climatological model biases, while allowing the model to generate internal variability and respond to radiative forcing. The CM2.1 and

125 FLOR models are used in routine seasonal prediction as part of the North American MultiModel
126 Ensemble (Kirtman et al. 2013).
127
128 We use several types of experiments. Experiments using CM2.1 are ten-member ensembles, while
129 experiments using FLOR and FLOR_FA are five-member ensembles
130 (1) CONTROL: These simulations use concentrations of greenhouse gases and other radiative forcing
131 components that are constant at preindustrial conditions (approximately calendar year 1860).
132 (2) CONTROL_STRESS: These simulations are conducted as departures from the Control simulation,
133 but in which a uniform zonal wind stress anomaly (-0.008 N m^{-2}) over a rectangular domain in the
134 Tropical Pacific is *added* to the momentum flux into the ocean calculated by the coupled model from
135 air-sea gradients. The domain for the stress addition extends from 15°S to 15°N, with a 10° buffer
136 zone on the northern and southern sides where the stress anomalies taper linearly to zero at +/- 25°
137 latitude; in longitude the domain extends from 150°E to the coast of South America, with a 10° buffer
138 zone from 140°E to 150°E. These simulations are 100 years long.
139 (3) ALLFORC: These simulations cover the period from 1861 to 2040, using estimates of the observed
140 changes in radiative forcing over the 1861-2005 period, and with estimated changes in radiative
141 forcing for 2006-2040 based on the Radiative Concentration Pathways scenario 4.5 (RCP4.5; see
142 http://cmip-pcmdi.llnl.gov/cmip5/forcing.html for details).
143 (4) ALLFORC_STRESS: These simulations are identical to ALLFORC, except that the model calculated
144 wind stress anomalies that the ocean feels are replaced over the tropical Pacific (region shown in Fig.
145 1b) with stress anomalies derived from European Center for Medium Range Weather Forecasting
146 (ECMWF) reanalysis (Dee et al. 2011) on a month by month basis over the period 1979-2013. This
147 replacement occurs only over the tropical Pacific, and only affects the momentum flux. The

differences between ALLFORC_STRESS and ALLFORC experiments represent the impacts on the global climate system of the momentum flux into the ocean from observed tropical Pacific wind stress anomalies over the period 1979-2013.

More specifically, we replace the model calculated wind stress at each time step with a stress value from an imposed wind stress time series. This time series is composed of three parts: (a) daily wind stress values from the ALLFORC simulation that have been filtered to retain only time scales shorter than 30 days, (b) a repeating seasonal cycle of wind stress calculated from the ALLFORC experiment, and (c) monthly wind stress perturbations derived from the ECMWF Interim Reanalysis (Dee et al. 2011). These perturbations are calculated as the anomalies from their climatological seasonal cycle computed over the 1979-2013 period - this ensures that the time-mean of the reanalysis wind stress anomalies applied to the CM2.1 model is zero over the 1979-2013 period. The above construction conserves the time-mean of the wind stress time series from the original coupled model, so as not to induce a model drift, but still allows the model to feel interannual wind stress variations similar to observational estimates over this period. For the Pacific there is a complete replacement of the wind stress in the deep Tropics (15^0S-15^0N); from 25^0S-15^0S and 15^0N-25^0N the wind stress is a mixture of the model's calculated wind stress and the replacement time series, with a linear taper such that the replacement effect goes to zero at 25^0S and 25^0N. Poleward of 25^0 the model stresses are computed entirely by the model based on air-sea gradients and then passed to the ocean component. In this process we only alter the flux of momentum through the stress field – the wind effects on latent and sensible heat fluxes are unaltered, and are computed based on the model's internal physics.

We show the time series (Fig. 1a) and spatial pattern (Fig. 1b) of the tropical Pacific wind stress anomalies imposed in the ALLFORC_STRESS experiments. The primary characteristic is an enhancement of the easterly winds from the late 1990s onward. The ALLFORC_STRESS simulations are able to largely replicate the observed timings of El Niño and La Niña events (Fig. 2) in response to the imposed wind stress anomalies, although the simulated amplitude of SST variations is larger than observed. The simulation of ENSO in FLOR_FA is notably more realistic than in FLOR (Vecchi et al. 2014), with a more realistic amplitude and seasonal phase locking than in FLOR or CM2.1.

We note that within the tropical Pacific, the zonal wind stress is tightly coupled to the zonal SST gradient and zonal thermocline slope. Thus in the above experiments, the wind stress can be viewed as a proxy for the state of the tropical Pacific ocean and atmosphere. Prescribing the wind stress anomalies in this region is one method to prescribe the full decadal state of the tropical Pacific, which then permits an assessment of the Pacific's downstream impacts on the rest of the globe.

b. Observational data

The observed monthly precipitation data(Harris et al. 2014) comes from the Climatic Research Unit (CRU) of the University of East Anglia. The data is global on a 0.5^0 grid, extending from 1901 through 2012. The observed monthly surface air temperature (HADCRU4) (Jones et al. 2012) also comes from CRU, and is on a 5^0 grid, extending from 1850 to the present. The surface wind stresses come from the European Center for Medium Range Weather Forecasting (ECMWF)-Interim Reanalysis(Dee et al. 2011).

3. Results

193 **a. Temperature response**

194 The simulations are able to capture many aspects of the hiatus in response to these winds (Fig. 3a).
195 The observed record shows the 2002-2013 hiatus period with little trend in global mean surface air
196 temperature. The ALLFORC ensemble continues warming throughout the period. In contrast, the
197 ALLFORC_STRESS ensemble has considerably reduced warming after the year 2002, demonstrating
198 that it has replicated aspects of the observed hiatus in response to the strengthening of the tropical
199 Pacific easterly winds, similar to England et al. (2014). While the ALLFORC_STRESS ensemble mean
200 warming trend is still larger than the observations (for CM2.1 and FLOR), the decadal temperature
201 trends in the ALLFORC_STRESS ensemble members using the three models are systematically smaller
202 than in the corresponding ALLFORC ensembles (Fig. 3b). In particular, the observed trend lies near
203 the center of the distribution of trends from the ALLFORC_STRESS runs using FLOR_FA.
204
205 We show in Fig. 4 the patterns of surface and subsurface ocean temperature change in response to the
206 imposed wind stress changes using the CM2.1 model for the ALLFORC_STRESS and CONTROL_STRESS
207 experiments (we obtain similar results using the FLOR and FLOR_FA models, not shown). By
208 increasing upwelling and vertical mixing, and strengthening the zonal tilt of the equatorial
209 thermocline, the enhanced easterly winds force cold, subsurface water in the eastern tropical Pacific
210 to the surface. The enhanced winds also depress the thermocline in the western tropical Pacific, and
211 force warm near-surface water in the tropical western Pacific to subduct into the ocean interior; this
212 leads to positive subsurface temperature anomalies in the western tropical Pacific (Figs. 4b and 4d).
213 The exposure of the cold water to the atmosphere in the eastern Pacific, combined with the
214 movement of warmer surface water into the subsurface ocean in the western Pacific, contributes to

215 the hiatus. In contrast, the pattern of SST change that occurs solely in response to radiative forcing
216 changes (Fig. 5) is much more uniform.

217 **b. Precipitation response**

218 How are these enhanced easterlies and the hiatus connected to North American drought? It has been
219 known for some time that SST in the Pacific can influence precipitation over North America
220 (Ropelewski and Halpert 1986; Trenberth et al. 1988; Hoerling 2003; Seager et al. 2005; Schubert et
221 al. 2004, 2009; Findell and Delworth 2010; Seager and Hoerling 2014; Wang and Schubert 2014b). In
222 particular, cold ocean temperature anomalies in the eastern tropical Pacific have been linked with
223 anomalously dry conditions over parts of North America. We therefore examine whether these stress-
224 induced Pacific SST changes induce precipitation anomalies over North America.

225

226 We first examine (Fig. 6) the ability of the models to simulate annual mean climatological
227 precipitation over North America. The higher resolution models (FLOR and FLOR_FA) simulate a
228 more realistic spatial pattern and magnitude of annual mean precipitation than the lower resolution
229 CM2.1 model. In addition, the model using flux adjustments (FLOR_FA) has the most realistic
230 simulation of annual mean precipitation among the models, including a more realistic depiction of the
231 east-west precipitation gradients from Texas through the Great Plains. Biases in the model's
232 simulation of ocean temperature contribute to the biases in continental precipitation over North
233 America (and for other continents, not shown).

234

235 We show in Figure 7 changes in annual mean precipitation (2002-2012 minus 1979-2000) for the
236 observations (Fig. 7a), and for the ALLFORC_STRESS simulations (Fig. 7b-d). The observed tendency
237 for reduced precipitation in western North America (Fig. 7a) is reproduced in the ALLFORC_STRESS

experiments with each model (Fig. 7b-d). Averaged over the region 130^0W-95^0W, and 30^0N-42^0N, the reduction in observed precipitation is 0.137 mm day^{-1}. For models CM2.1, FLOR, and FLOR_FA the simulated reductions over this region (land only) are 0.102, 0.095, and 0.117 mm day^{-1}, respectively. Since these experiments contain both radiative forcing changes and wind stress changes, we ask whether the tendency for reduced precipitation is due to radiative forcing changes or to the effects of tropical Pacific wind stress changes. We estimate the wind-forced component as the difference in precipitation between the ALLFORC_STRESS and ALLFORC experiments for the 2002-2012 period. We also estimate the radiatively forced component as the precipitation in ALLFORC for the 2002-2012 period minus the 1979-2000 period. Combining the results of all three models, the wind-stress forcing accounts for 92% of the reduction in simulated annual mean precipitation, with the radiatively forced component accounting for 8%. A number of model-based studies (see, for example, (Seager et al. 2007; Cayan et al. 2010)) have shown that aridity may increase over southwestern North America in response to increasing greenhouse gases and the resultant warming of the planet, and from associated factors such as the expansion of the Hadley cell(Lu et al. 2007). However, the current results suggest that such factors were not primary drivers of the recent drought, consistent with earlier results (Hoerling et al. 2010; Seager and Naik 2012).

The tropical SST anomaly pattern creates a tendency for an atmospheric circulation pattern that is conducive to drought, but atmospheric internal dynamics also influence whether or not a drought occurs. Given this important role for atmospheric internal variability, we evaluate the likelihood of a change in precipitation in a more probabilistic framework. We first note that for the period 1979-2000 we have 220 individual years for the CM2.1 ALLFORC ensemble (22 years times ten ensemble members), and 220 total years for the ALLFORC ensembles using both FLOR and FLOR_FA (22 years

261 times five ensemble members times two models). For each model time series we compute an areal
262 mean over the region 130^0W-95^0W and 30^0N-42^0N (land only). We consider all of the model output
263 for the period 1979-2000 to be one "population" (440 points). We then randomly sample this
264 population, drawing eleven samples at a time and then computing an eleven-year mean (the same
265 length as the 2002-2012 period). We repeat this process 10,000 times to form a distribution of
266 decadal mean precipitation anomalies consistent with the 1979-2000 period for these models, and
267 show that in Figure 8 as a cumulative distribution function. We do the same with output from the
268 ALLFORC_STRESS ensembles over this same period. These two distributions are very similar,
269 indicating similar likelihoods of dry and wet decades from the ALLFORC and ALLFORC_STRESS
270 ensembles for the 1979-2000 period. We then repeat this process using output for the period 2002-
271 2012 from the ALLFORC ensemble. We see (Fig. 8) that the distribution for 2002-2012 from the
272 ALLFORC ensemble has been displaced slightly to the left, indicating a small increased likelihood of
273 negative decadal-mean precipitation anomalies in response to radiative forcing changes. We next
274 repeat this process for the ALLFORC_STRESS output from 2002-2012. We find a much larger
275 movement of the distribution to the left, indicating a substantial increase in the likelihood of dry
276 decades in response to enhanced tropical easterly winds. It is still quite possible to have a decade with
277 above average precipitation in the ALLFORC_STRESS simulations, but the likelihood of such a decade
278 has dropped substantially. These model results therefore suggest that the sustained easterly wind
279 anomalies over the tropical Pacific, through their relationship with local sea surface temperature,
280 created conditions that greatly increased the likelihood of drought over parts of western North
281 America over the last decade, with an additional smaller role for radiative forcing changes in these
282 models.
283

We find through examination of multi-millennial control simulations that the magnitude and duration of the easterly wind stress anomaly seen over the last decade in the tropical Pacific is unprecedented based on this model's control run internal variability, consistent with England et al (2014). This suggests several possibilities – (i) the models do not simulate sufficient decadal-scale internal variability, (ii) the observed event over the last decade is so rare that longer model simulations would be needed to realize such an event, or (iii) or the easterly wind stress anomaly has some contribution from radiative forcing that is not dominant in these models (Clement et al. 1996; Compo and Sardeshmukh 2009; Solomon and Newman 2012).

4. Discussion and potential future changes

The strong connection between the intensification of Pacific trades and the drying in western North America observed over the past decade suggests that this drying cannot be connected in a straightforward fashion to greenhouse gas increases. In most coupled GCM simulations anthropogenic forcing produces a long-term *weakening* of the Walker circulation and tropical Pacific trade winds, but with substantial intrinsically-generated variability on decadal scales(Vecchi et al. 2006). Therefore, unless it can be shown that the strengthened trade winds are a result of either natural or human-induced radiative forcing changes, the model results suggest that the observed drying over the western U.S. over the last decade may be primarily due to natural variability, and therefore not necessarily a harbinger of a secular drying trend (Hoerling et al. 2010; Seager and Naik 2012). These results highlight how vulnerable western North America is to severe decadal swings in hydroclimate arising from internal variations of the climate system. Recent results suggest that temperature variations in either the Indian Ocean (Luo et al. 2012) or the Atlantic Ocean (McGregor et

306 al. 2014) could act as external drivers of, or feedbacks for, the Pacific trade wind changes. It is also
307 possible that the wind changes are due solely to coupled processes in the tropical Pacific.
308
309 To illustrate possible changes in drought over the next decade we conduct two additional
310 experiments for the period 2014-2022 using CM2.1, both starting from the end of the
311 ALLFORC_STRESS experiment. In the first experiment we do not impose wind stress anomalies, and
312 the model computes its own wind stresses for the 2014-2022 period. In the second experiment the
313 model experiences the same sequence of wind stress anomalies that was experienced over 2005-2013
314 (ie, with unusually strong easterly winds). In the first experiment (Fig. 9a) precipitation is much
315 closer to its climatological normal, with interannual deviations around the long-term mean. In the
316 second experiment (Fig. 9b) there is a tendency for continued negative precipitation anomalies over
317 the western U.S. in response to the continued easterly wind stress anomalies in the tropical Pacific.
318 Therefore, a significant factor over the coming decade for western U.S. water resources, and for the
319 water managers dealing with variations in water supply, is the behavior of the winds in the tropical
320 Pacific. Although prediction of such decadal-scale variations is challenging (Wittenberg et al. 2014), it
321 is important to improve our understanding of the factors responsible for the wind stress anomalies
322 observed over 2002-2013(McGregor et al. 2014). This may allow us to better characterize potential
323 future trajectories for western U.S. water resources.
324
325 We further assess future prospects for the hiatus and North American drought using the idealized
326 experiment CONTROL_STRESS. In this experiment we maintain the idealized zonal wind stress forcing
327 anomaly for 100 years, and assess the evolution of the climate system. We see (Fig. 10a) that the
328 global cooling in response to the enhanced tropical easterlies is a transient feature, persisting in these

models for only a decade or two. In these simulations the initial cooling is associated with upwelling of cold subsurface water and subduction of warmer surface water into the interior. We find that after a decade or two some of this warmer water that was sequestered in the ocean interior makes its way back to the surface (Fig. 11), offsetting the cooling associated with upwelling in the eastern tropical Pacific, and therefore eliminating the global cooling signal. There is in fact a small tendency for positive global temperature anomalies, likely associated with enhanced oceanic heat uptake during the first decade or two of these simulations. In contrast, eastern tropical Pacific SST anomalies remain negative, although with somewhat reduced amplitude. These results suggest that if the hiatus in global warming is generated solely by enhanced tropical wind stress, then the duration of the hiatus is limited to of order a decade or two (at least according to this model). This time scale is determined by the processes by which positive heat anomalies that were sequestered in the upper tropical ocean can reemerge at the surface. However, despite the elimination of the global cooling, negative temperature anomalies persist in the eastern tropical Pacific (Fig. 10b), and therefore continue to create conditions conducive to drought over western North America (Fig. 10c), although with diminishing amplitude. This suggests that the drought would persist in response to a continued surface cooling in the eastern tropical Pacific, despite the cessation of the hiatus in global warming.

Acknowledgements

We thank Drs. H. Murakami and X. Yang, along with three anonymous reviewers, for very helpful comments on earlier versions of this manuscript. HADCRU4 temperature data,were provided by the NOAA/OAR/ESRL PSD, Boulder, Colorado, USA, from their Web site at http://www.esrl.noaa.gov/psd. ECMWF-Interim reanalysis data was downloaded from http://apps.ecmwf.int/datasets/data/interim_full_moda/.

353 References

354

355 Balmaseda, M. A., K. E. Trenberth, and E. Källén, 2013: Distinctive climate signals in reanalysis of
356 global ocean heat content: SIGNALS IN OCEAN HEAT CONTENT. *Geophys. Res. Lett.*, **40**, 1754–
357 1759, doi:10.1002/grl.50382.

358 Bindoff, N.L., et al., 2013: *Detection and Attribution of Climate Change: from Global to Regional.*
359 Cambridge University Press, Cambridge, United Kingdom and New York, NY, USA.,.

360 Cayan, D. R., T. Das, D. W. Pierce, T. P. Barnett, M. Tyree, and A. Gershunov, 2010: Future dryness in
361 the southwest US and the hydrology of the early 21st century drought. *Proc. Natl. Acad. Sci.*,
362 **107**, 21271–21276.

363 Clement, A., and P. DiNezio, 2014: The Tropical Pacific Ocean--Back in the Driver's Seat? *Science*, **343**,
364 976–978, doi:10.1126/science.1248115.

365 ——, R. Seager, M.A. Cane, and S.E. Zebiak, 1996: An ocean dynamical thermostat. *J. Clim.*, **9**, 2190–
366 2196.

367 Compo, G. P., and P. D. Sardeshmukh, 2009: Removing ENSO-Related Variations from the Climate
368 Record. *J. Clim.*, **23**, 1957–1978, doi:10.1175/2009JCLI2735.1.

369 Cowtan, K., and R. G. Way, 2014: Coverage bias in the HadCRUT4 temperature series and its impact on
370 recent temperature trends: Coverage Bias in the HadCRUT4 Temperature Series. *Q. J. R.*
371 *Meteorol. Soc.*, n/a – n/a, doi:10.1002/qj.2297.

372 Dee, D. P., and Coauthors, 2011: The ERA-Interim reanalysis: configuration and performance of the
373 data assimilation system. *Q. J. R. Meteorol. Soc.*, **137**, 553–597, doi:10.1002/qj.828.

374 Delworth, T. L., and Coauthors, 2006: GFDL's CM2 global coupled climate models. Part I: Formulation
375 and simulation characteristics. *J. Clim.*, **19**.

376 ——, and Coauthors, 2012: Simulated Climate and Climate Change in the GFDL CM2.5 High-Resolution
377 Coupled Climate Model. *J. Clim.*, **25**, 2755–2781, doi:10.1175/JCLI-D-11-00316.1.

378 Dennison, P. E., S. C. Brewer, J. D. Arnold, and M. A. Moritz, 2014: Large wildfire trends in the western
379 United States, 1984-2011: Dennison et al.; Large wildfire trends in the western US. *Geophys.*
380 *Res. Lett.*, **41**, 2928–2933, doi:10.1002/2014GL059576.

381 Easterling, D. R., and M. F. Wehner, 2009: Is the climate warming or cooling? *Geophys. Res. Lett.*, **36**,
382 doi:10.1029/2009GL037810. http://doi.wiley.com/10.1029/2009GL037810 (Accessed
383 November 12, 2014).

384 England, M. H., and Coauthors, 2014: Recent intensification of wind-driven circulation in the Pacific
385 and the ongoing warming hiatus. *Nat. Clim. Change*, **4**, 222–227, doi:10.1038/nclimate2106.

386 Findell, K. L., and T. L. Delworth, 2010: Impact of Common Sea Surface Temperature Anomalies on
387 Global Drought and Pluvial Frequency. *J. Clim.*, **23**, 485–503, doi:10.1175/2009JCLI3153.1.

388 Funk, C., A. Heoll, and D. Stone, 2014: Examining the contribution of the observed global warming
389 trend to the California droughts of 2012/2013 and 2013/2014. *Bull Amer Meteor Soc*, **95**, S11–
390 S15.

Harris, I., P. D. Jones, T. J. Osborn, and D. H. Lister, 2014: Updated high-resolution grids of monthly climatic observations - the CRU TS3.10 Dataset: UPDATED HIGH-RESOLUTION GRIDS OF MONTHLY CLIMATIC OBSERVATIONS. *Int. J. Climatol.*, **34**, 623–642, doi:10.1002/joc.3711.

Hawkins, E., T. Edwards, and D. McNeall, 2014: Pause for thought. *Nat. Clim. Change*, **4**, 154–156.

Hoerling, M., 2003: The Perfect Ocean for Drought. *Science*, **299**, 691–694, doi:10.1126/science.1079053.

Hoerling, M., J. Eischeid, and J. Perlwitz, 2010: Regional Precipitation Trends: Distinguishing Natural Variability from Anthropogenic Forcing. *J. Clim.*, **23**, 2131–2145, doi:10.1175/2009JCLI3420.1.

Jones, P. D., D. H. Lister, T. J. Osborn, C. Harpham, M. Salmon, and C. P. Morice, 2012: Hemispheric and large-scale land-surface air temperature variations: An extensive revision and an update to 2010. *J. Geophys. Res.*, **117**, doi:10.1029/2011JD017139. http://doi.wiley.com/10.1029/2011JD017139 (Accessed April 29, 2014).

Katsman, C. A., and G. J. van Oldenborgh, 2011: Tracing the upper ocean's "missing heat": TRACING THE UPPER OCEAN'S "MISSING HEAT." *Geophys. Res. Lett.*, **38**, n/a – n/a, doi:10.1029/2011GL048417.

Kirtman, B. P., and Coauthors, 2013: The North American Multi-Model Ensemble (NMME): Phase-1 seasonal to interannual prediction, phase-2 toward developing intra-seasonal prediction. *Bull. Am. Meteorol. Soc.*,. http://journals.ametsoc.org/doi/abs/10.1175/BAMS-D-12-00050.1 (Accessed November 7, 2014).

410 Kosaka, Y., and S.-P. Xie, 2013: Recent global-warming hiatus tied to equatorial Pacific surface cooling.
411 *Nature*, **501**, 403–407, doi:10.1038/nature12534.

412 Lu, J., G. A. Vecchi, and T. Reichler, 2007: Expansion of the Hadley cell under global warming. *Geophys.*
413 *Res. Lett.*, **34**, doi:10.1029/2006GL028443. http://doi.wiley.com/10.1029/2006GL028443
414 (Accessed November 12, 2014).

415 Luo, J.-J., W. Sasaki, and Y. Masumoto, 2012: Indian Ocean warming modulates Pacific climate change.
416 *Proc. Natl. Acad. Sci.*, **109**, 18701–18706, doi:10.1073/pnas.1210239109.

417 Magnusson, L., M. Alonso-Balmaseda, and F. Molteni, 2013: On the dependence of ENSO simulation on
418 the coupled model mean state. *Clim. Dyn.*, **41**, 1509–1525, doi:10.1007/s00382-012-1574-y.

419 McGregor, S., A. Timmermann, M. F. Stuecker, M. H. England, M. Merrifield, F.-F. Jin, and Y. Chikamoto,
420 2014: Recent Walker circulation strengthening and Pacific cooling amplified by Atlantic
421 warming. *Nat. Clim. Change*, doi:10.1038/nclimate2330.
422 http://www.nature.com/doifinder/10.1038/nclimate2330 (Accessed August 4, 2014).

423 Meehl, G. A., J. M. Arblaster, J. T. Fasullo, A. Hu, and K. E. Trenberth, 2011: Model-based evidence of
424 deep-ocean heat uptake during surface-temperature hiatus periods. *Nat. Clim. Change*, **1**, 360–
425 364, doi:10.1038/nclimate1229.

426 ——, A. Hu, J. M. Arblaster, J. Fasullo, and K. E. Trenberth, 2013: Externally Forced and Internally
427 Generated Decadal Climate Variability Associated with the Interdecadal Pacific Oscillation. *J.*
428 *Clim.*, **26**, 7298–7310, doi:10.1175/JCLI-D-12-00548.1.

Ogata, T., S.-P. Xie, A. Wittenberg, and D.-Z. Sun, 2013: Interdecadal Amplitude Modulation of El Niño–Southern Oscillation and Its Impact on Tropical Pacific Decadal Variability*. *J. Clim.*, **26**, 7280–7297, doi:10.1175/JCLI-D-12-00415.1.

Ropelewski, C., and M. Halpert, 1986: North American Precipitation and Temperature Patterns Associated with the El Nino/Southern Oscillation (ENSO). *Mon. Weather Rev.*, **114**, 2352–2362.

Santer, B. D., and Coauthors, 2014: Volcanic contribution to decadal changes in tropospheric temperature. *Nat. Geosci.*, **7**, 185–189, doi:10.1038/ngeo2098.

Schubert, S., and Coauthors, 2009: A US CLIVAR project to assess and compare the responses of global climate models to drought-related SST forcing patterns: Overview and results. *J. Clim.*, **22**.

Schubert, S. D., M. J. Suarez, P. J. Pegion, R. D. Koster, and J. T. Bacmeister, 2004: Causes of long-term drought in the US Great Plains. *J. Clim.*, **17**.

Seager, R., and N. Naik, 2012: A Mechanisms-Based Approach to Detecting Recent Anthropogenic Hydroclimate Change*. *J. Clim.*, **25**, 236–261, doi:10.1175/JCLI-D-11-00056.1.

——, and M. Hoerling, 2014: Atmosphere and Ocean Origins of North American Droughts. *J. Clim.*, 140404144919009, doi:10.1175/JCLI-D-13-00329.1.

——, Y. Kushnir, C. Herweijer, N. Naik, and J. Velez, 2005: Modeling of tropical forcing of persistent droughts and pluvials over western North America: 1856–2000. *J. Clim.*, **18**.

Seager, R., and Coauthors, 2007: Model Projections of an Imminent Transition to a More Arid Climate in Southwestern North America. *Science*, **316**, 1181–1184, doi:10.1126/science.1139601.

448 Seager, R., M. Hoerling, H. Wang, B. Lyon, A. Kumar, J. Nakamura, and N. Henderson, 2015: Causes and
449 predictability of the 2011-2014 California drought. *J. Clim.*, doi:Submitted.

450 Solomon, A., and M. Newman, 2012: Reconciling disparate twentieth-century Indo-Pacific ocean
451 temperature trends in the instrumental record. *Nat. Clim Change*, **2**, 691–699,
452 doi:10.1038/nclimate1591.

453 Solomon, S., K. H. Rosenlof, R. W. Portmann, J. S. Daniel, S. M. Davis, T. J. Sanford, and G.-K. Plattner,
454 2010: Contributions of Stratospheric Water Vapor to Decadal Changes in the Rate of Global
455 Warming. *Science*, **327**, 1219–1223, doi:10.1126/science.1182488.

456 Stahle, D. W., E. R. Cook, J. V. Diaz, F. K. Fye, D. J. Burnette, R. A. Soto, R. Seager, and R. R. Heim, 2009:
457 Early 21st-century drought in Mexico. *Eos Trans. Am. Geophys. Union*, **90**, 89–90.

458 Swain, D., M. Tsiang, M. Haugen, D. Singh, A. Charland, B. Rajaratnam, and N. Diffenbaugh, 2014: The
459 extraordinary California drought of 2013/14; character, context, and the role of climate
460 change. *Bull Amer Meteor Soc*, **95**, S3–S7.

461 Trenberth, K. E., and J. T. Fasullo, 2013: An apparent hiatus in global warming? *Earths Future*, **1**, 19–
462 32, doi:10.1002/2013EF000165.

463 ——, G. W. Branstator, and P. A. Arkin, 1988: Origins of the 1988 North American Drought. *Science*,
464 **242**, 1640–1645, doi:10.1126/science.242.4886.1640.

465 Tung, K.-K., and J. Zhou, 2013: Using data to attribute episodes of warming and cooling in
466 instrumental records. *Proc. Natl. Acad. Sci.*, **110**, 2058–2063, doi:10.1073/pnas.1212471110.

467 Vecchi, G. A., and A. T. Wittenberg, 2010: El Niño and our future climate: where do we stand? *Wiley*
468 *Interdiscip. Rev. Clim. Change*, n/a – n/a, doi:10.1002/wcc.33.

469 ——, B. J. Soden, A. T. Wittenberg, I. M. Held, A. Leetmaa, and M. J. Harrison, 2006: Weakening of
470 tropical Pacific atmospheric circulation due to anthropogenic forcing. *Nature*, **441**, 73–76,
471 doi:10.1038/nature04744.

472 Vecchi, G. A., and Coauthors, 2014: On the Seasonal Forecasting of Regional Tropical Cyclone Activity.
473 *J. Clim.*, **27**, 7994–8016, doi:10.1175/JCLI-D-14-00158.1.

474 Wang, H., and S. Schubert, 2014a: Causes of the extreme dry conditions over California during early
475 2013. *Bull Amer Meteor Soc*, **95**, S7–S11.

476 ——, and ——, 2014b: The Precipitation Response over the Continental United States to Cold Tropical
477 Pacific Sea Surface Temperatures. *J. Clim.*, 140408145639001, doi:10.1175/JCLI-D-13-00453.1.

478 Wittenberg, A. T., A. Rosati, N.-C. Lau, and J. J. Ploshay, 2006: GFDL's CM2 global coupled climate
479 models. Part III: Tropical Pacific climate and ENSO. *J. Clim.*, **19**.

480 ——, ——, T. L. Delworth, G. A. Vecchi, and F. Zeng, 2014: ENSO Modulation: Is It Decadally
481 Predictable? *J. Clim.*, **27**, 2667–2681, doi:10.1175/JCLI-D-13-00577.1.

Figures

Figure 1 (a) Time series of annual mean zonal wind stress applied to the model ocean in the "ALLFORC_STRESS" experiment averaged over 140^0E-160^0W, 15^0S-15^0N. Units are N m^{-2}. As discussed in the main text the stress values are from the ERA-Interim Reanalysis. (b) Spatial pattern of stress anomalies applied to model in "ALLFORC_STRESS" experiment for the period 2002-2012 relative to the period 1979-2000.

Figure 2 Time-longitude plots of monthly SST anomalies for observations (upper right, from the HADISST data set, Rayner et al., 2003) and models (CM2.1, FLOR, and FLOR_FA). SST values are averaged between 5^oS and 5^oN. Units are K. For visual perspective, dashed green lines are drawn every 10 years.

Figure 3 (a) Time series of anomalies in global mean, annual mean surface air temperature relative to the time-mean over the period 1951-1980. Units are K. Black line denotes observations from the Climatic Research Unit (CRU) at the University of East Anglia. Red (blue) line corresponds to the ensemble mean of the CM2.1 ALLFORC (ALLFORC_STRESS) experiments. A three-year running mean was applied to all time series. (b) Trends in global mean surface air temperature over the period 2000-2012, expressed as K $decade^{-1}$. Red (blue) symbols for ALLFORC (ALLFORC_STRESS) experiments. Large symbols are ensemble mean, small symbols are individual ensemble members. Experiments using models CM2.1, FLOR, and FLOR_FA are indicated by diamonds, circles, and squares respectively.

Figure 4 (a) Spatial pattern of the SST response to imposed wind stress forcing, calculated as the time-mean over 2002-2012 in ALLFORC_STRESS minus ALLFORC. (b) Same as (a) for temperature at 200m. Units are K for both panels. (c) Same as (a), but for experiment CONTROL_STRESS minus CONTROL. (d) Same as (b), but for experiment CONTROL_STRESS minus CONTROL.

Figure 5 Estimate of SST response(units are K) to radiative forcing change using the ALLFORC experiment with the CM2.1 model. The estimate is calculated as the 10-member ensemble mean SST for the 2002-2012 period minus the 10-member ensemble mean SST for the 1979-2000 period. The negative values in the subpolar North Atlantic are associated with a weakening of the Atlantic Meridional Overturning Circulation.

Figure 6 Precipitation climatology from observations and the models. Annual-mean precipitation is shown, units are mm day^{-1}. (a) Observations from Climatic Research Unit, University of East Anglia. (b) CM2.1 model. (c) FLOR_FA model, (d) FLOR model.

Figure 7 (a) Difference in observed annual mean precipitation for the period 2002-2012 minus 1979-2000. Observations from the Climatic Research Unit of the University of East Anglia. Units are mm day^{-1}. (b) Same as (a) using model results from CM2.1 ALLFORC_STRESS, showing the combined effects of wind stress and radiative forcing changes. (c) Same as (b) using FLOR_FA. (d) Same as (b) using FLOR.

Figure 8 Cumulative probability distribution of 11-year mean precipitation anomalies (mm day^{-1}) averaged over 130^0W-95^0W, 30^0N-42^0N, land only. Grey curve (black crosses) indicates results using model values from the period 1979-2000 from experiment ALLFORC (ALLFORC_STRESS) using all three models (CM2.1, FLOR, FLOR_FA). Red (blue) curve denotes values from ALLFORC (ALLFORC_STRESS) over the period 2002-2012. The distributions are generated by resampling all ensemble members from each model (CM2.1, FLOR, FLOR_FA) for the experiment and period indicated. For example, for the grey curve we use output from all ten ensemble members of experiment ALLFORC, as well as five ensemble members each from FLOR and FLOR_FA, over the period 1979-2000 (440 total points, based on 22 years and 10 ensemble members from CM2.1, and 5 ensemble members for 22 years for FLOR and FLOR_FA respectively). We randomly pick 11 different values from among this pool of 440 values, and then average those to form an 11-year mean, and then subtract from that the ensemble mean value over the period 1979-2000. We repeat this process 10,000 times to form a distribution of 11-year mean anomalies, and plot that as a cumulative probability distribution function. We repeat this process using years 1979-2000 from ALLFORC_STRESS, years 2002-2012 from ALLFORC, and years 2002-2012 from ALLFORC_STRESS.

Figure 9 Time series of simulated percentage change in annual mean precipitation relative to the 1979-2000 time-mean, spatially averaged over 130^oW-90^oW, 30^oN-42^oN (land only). The simulations used the CM2.1 model, were 10-member ensembles, and started from identical initial conditions at the end of experiment ALLFORC_STRESS. (a) Precipitation change with no wind forcing anomaly in tropical Pacific. (b) Precipitation change when observed wind stress anomalies over the period 2005-2013 are applied to the model over the period 2014-2022.

Figure 10 Response of temperature and precipitation to sustained addition of anomalous easterly wind stress in the tropical Pacific for experiment CONTROL_STRESS. (a) Time series of global mean surface air temperature response, calculated as global mean temperature in CONTROL_STRESS minus CONTROL. (b) Same as (a), but for SST averaged over a portion of the tropical eastern Pacific (170°W-100°W, 10°S-10°N). (c) Same as (a), but for annual mean rainfall averaged over 130°W-90°W, 30°N-42°N, land areas only, expressed as percentage change from long-term mean.

Figure 11 Response of global mean ocean temperature to sustained addition of anomalous easterly wind stress in the tropical Pacific, calculated as experiment CONTROL_STRESS - CONTROL. Positive values indicate a warming of the ocean in response to the anomalous easterlies.

Rendered Figure 1
Click here to download Rendered Figure: figures latest_v3 1.pdf

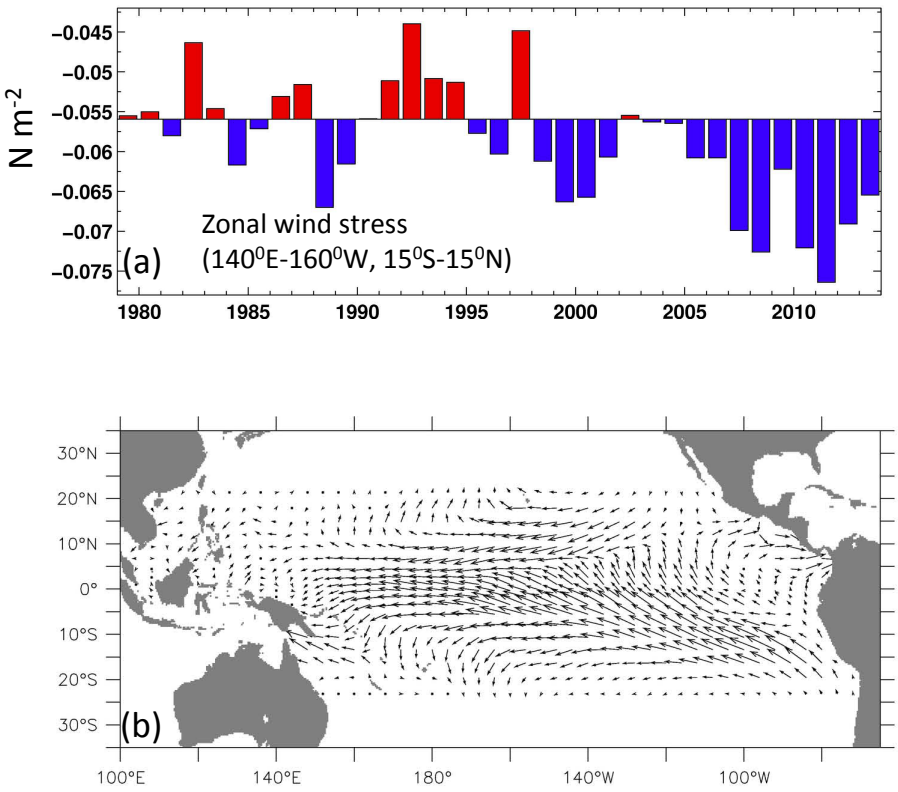

Figure 1 (a) Time series of annual mean zonal wind stress applied to the model ocean in the "ALLFORC_STRESS" experiment averaged over 140^{0}E-160^{0}W, 15^{0}S-15^{0}N. Units are N m^{-2}. As discussed in the main text the stress values are derived by combining the model's climatological seasonal cycle with the interannual anomalies from the ERA-Interim Reanalysis. (b) Spatial pattern of stress anomalies applied to model in "ALLFORC_STRESS" experiment for the period 2002-2012 relative to the period 1979-2000.

Rendered Figure 2

Click here to download Rendered Figure: figures latest_v3 2.pdf

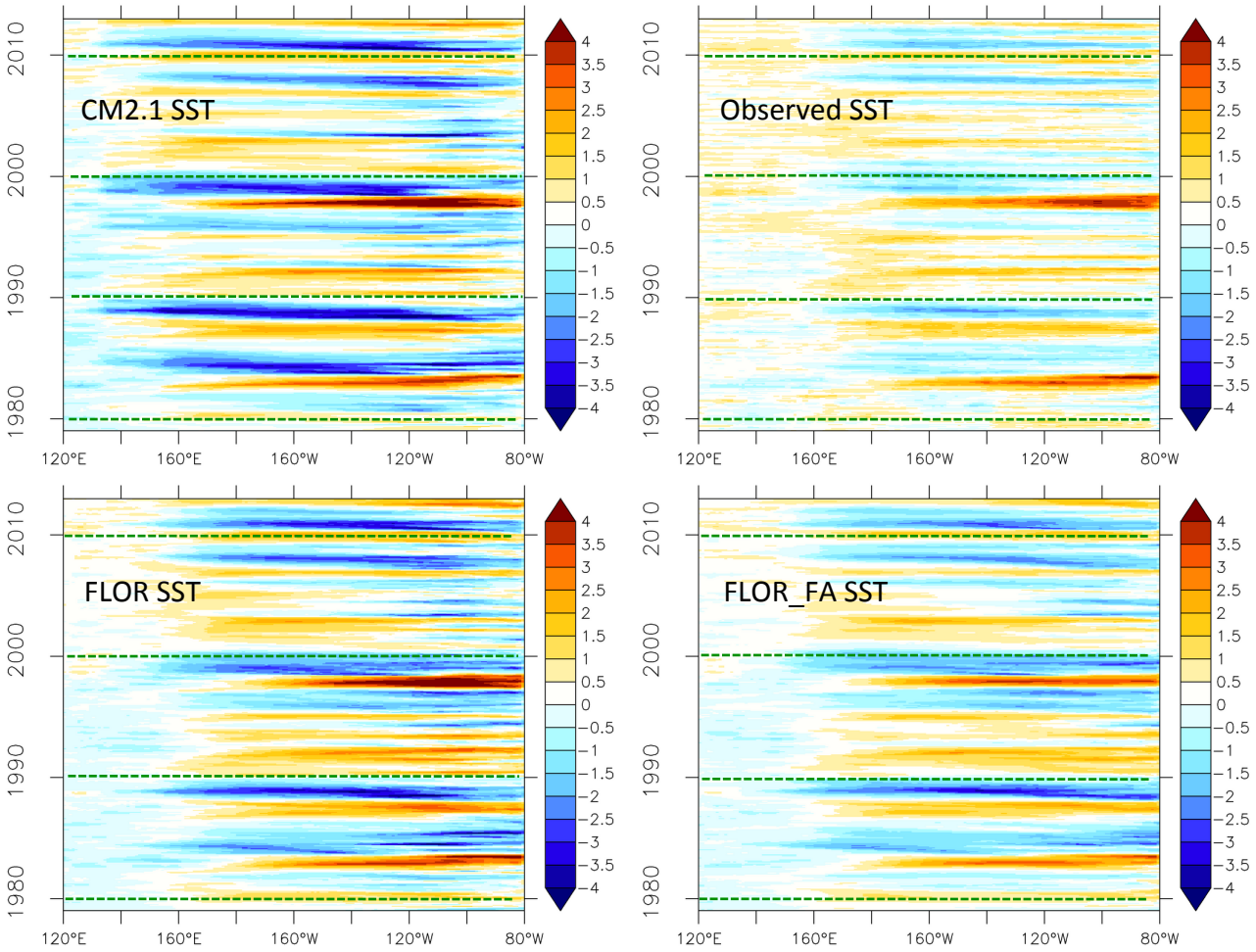

Figure 2 Time-longitude plots of monthly SST anomalies for observations (upper right, from the HADISST data set, Rayner et al., 2003) and models (CM2.1, FLOR, and FLOR_FA). SST values are averaged between 5ºS and 5ºN. Units are K. For visual perspective, dashed green lines are drawn every 10 years.

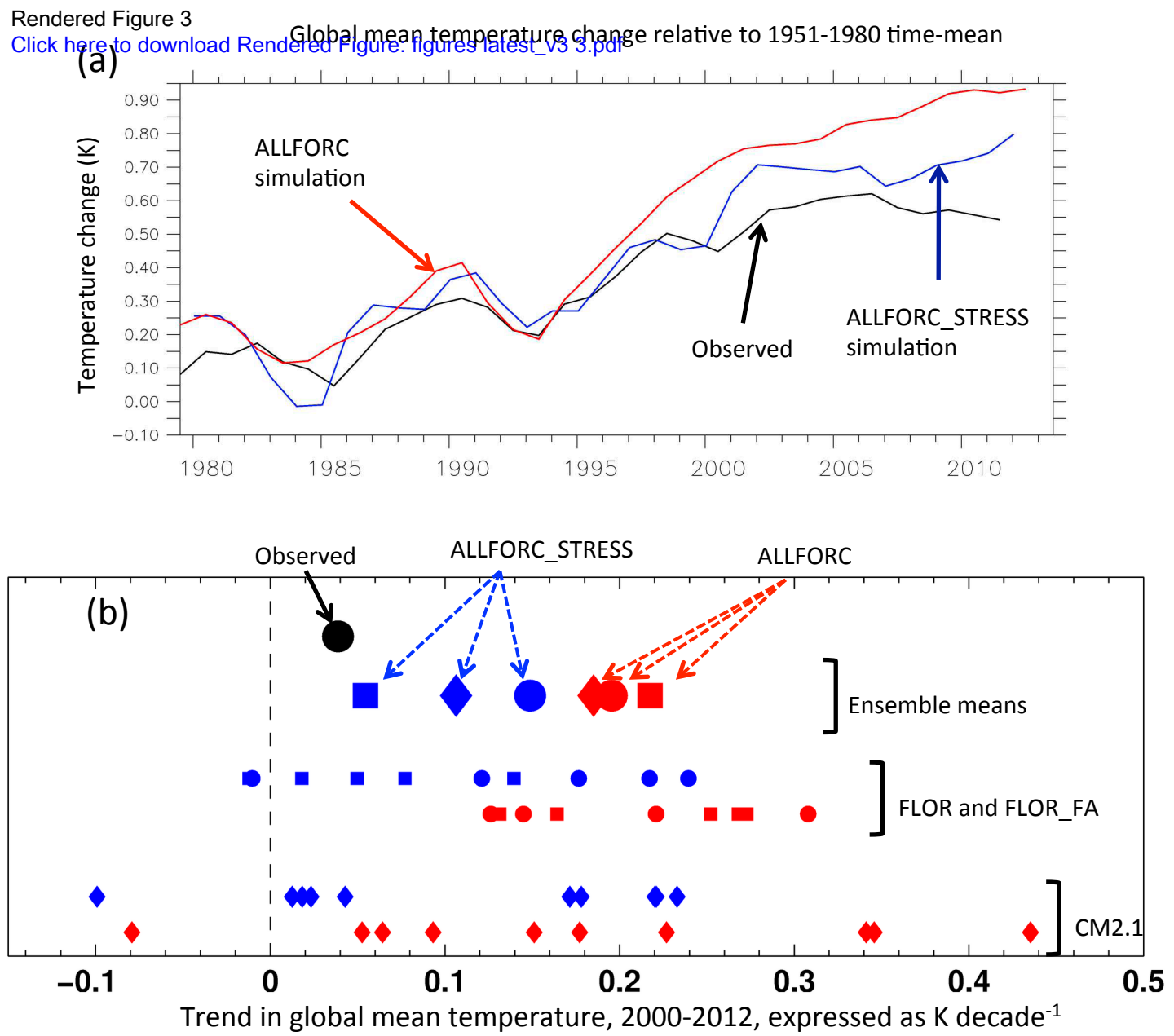

Figure 3 (a) Time series of anomalies in global mean, annual mean surface air temperature relative to the time-mean over the period 1951-1980. Units are K. Black line denotes observations from the Climatic Research Unit (CRU) at the University of East Anglia. Red (blue) line corresponds to the ensemble mean of the CM2.1 ALLFORC (ALLFORC_STRESS) experiments. A three-year running mean was applied to all time series. (b) Trends in global mean surface air temperature over the period 2000-2012, expressed as K decade^{-1}. Red (blue) symbols for ALLFORC (ALLFORC_STRESS) experiments. Large symbols are ensemble mean, small symbols are individual ensemble members. Experiments using models CM2.1, FLOR, and FLOR_FA are indicated by diamonds, circles, and squares respectively.

Rendered Figure 4
Click here to download Rendered Figure: figures latest_v3 4.pdf

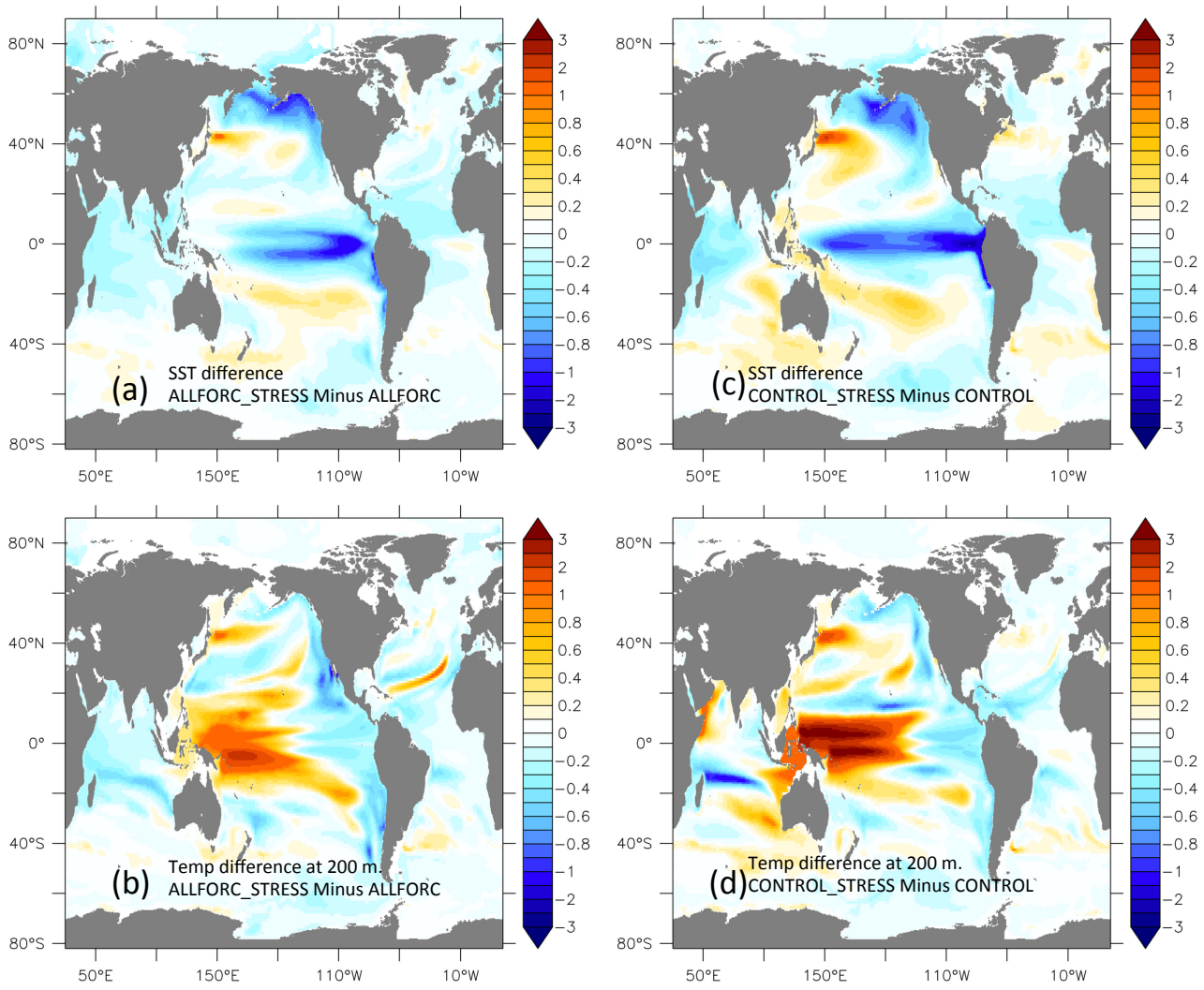

Figure 4 (a) Spatial pattern of the SST response to imposed wind stress forcing, calculated as the time-mean over 2002-2012 in ALLFORC_STRESS minus ALLFORC. (b) Same as (a) for temperature at 200m. Units are K for both panels. (c) Same as (a), but for experiment CONTROL_STRESS minus CONTROL. (d) Same as (b), but for experiment CONTROL_STRESS minus CONTROL.

Rendered Figure 5
Click here to download Rendered Figure: figures latest_v3 5.pdf

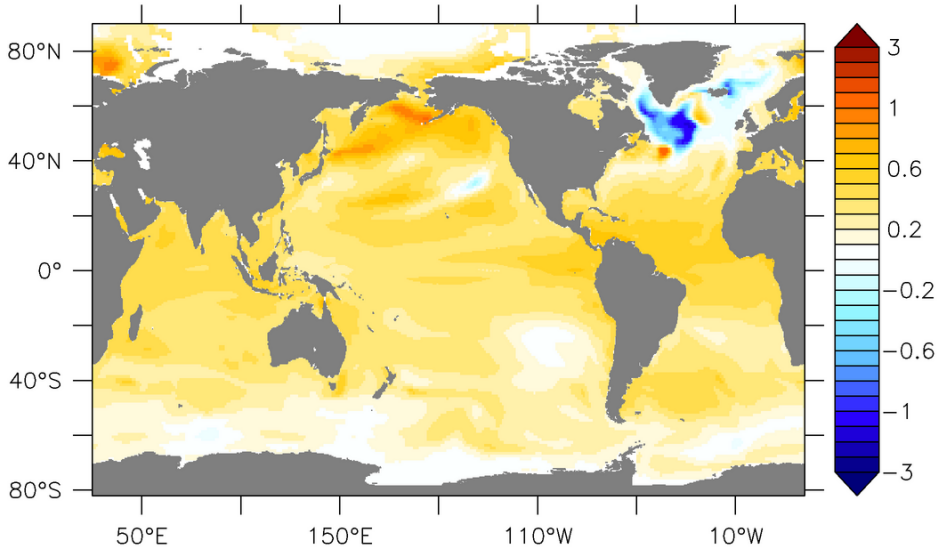

Figure 5 Estimate of SST response(units are K) to radiative forcing change using the ALLFORC experiment with the CM2.1 model. The estimate is calculated as the 10-member ensemble mean SST for the 2002-2012 period minus the 10-member ensemble mean SST for the 1979-2000 period. The negative values in the subpolar North Atlantic are associated with a weakening of the Atlantic Meridional Overturning Circulation.

Rendered Figure 6
Click here to download Rendered Figure: figures latest_v3 6.pdf

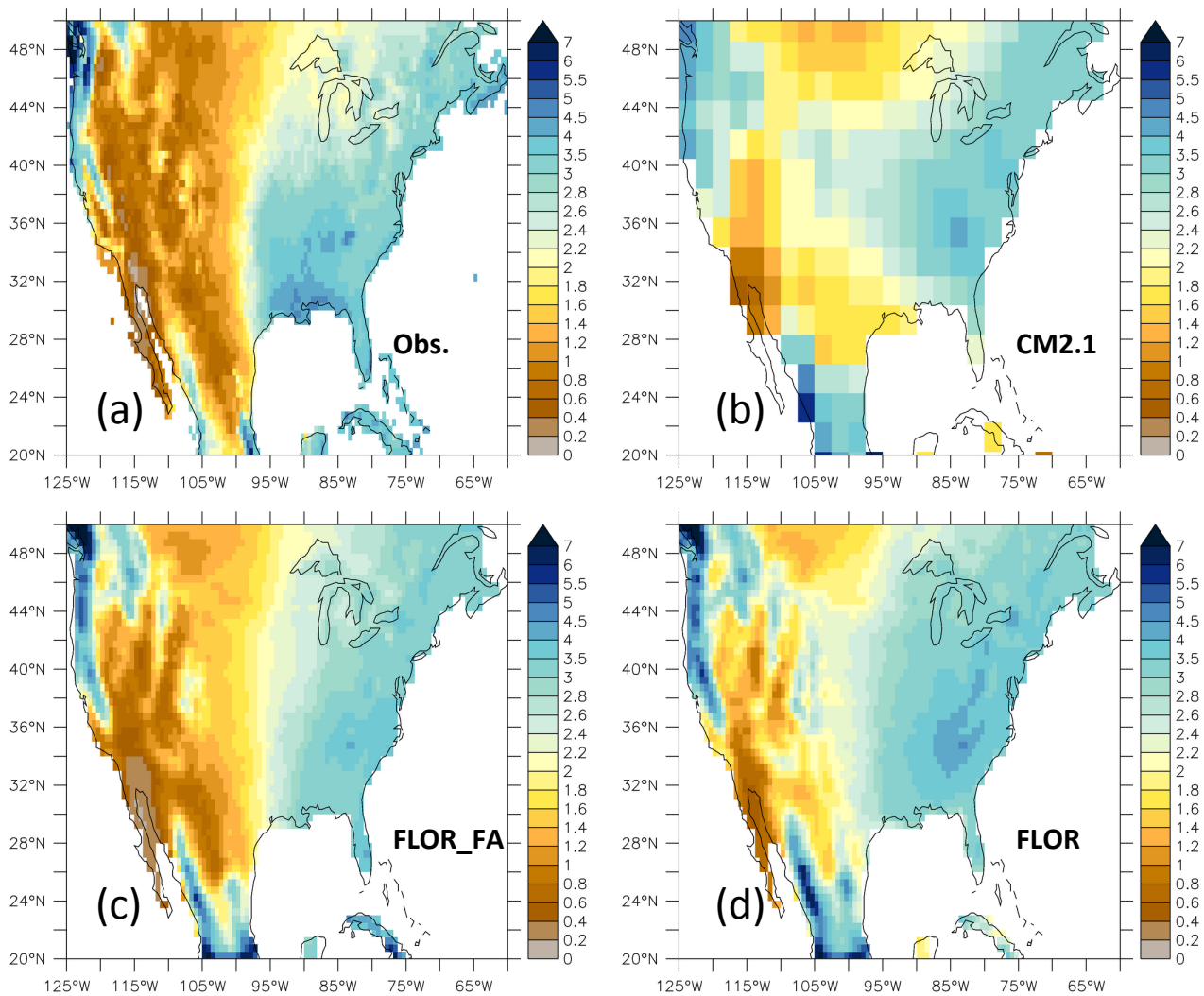

Figure 6 Precipitation climatology from observations and the models. Annual-mean precipitation is shown, units are mm day^{-1}. (a) Observations from Climatic Research Unit, University of East Anglia. (b) CM2.1 model. (c) FLOR_FA model, (d) FLOR model.

Rendered Figure 7
Click here to download Rendered Figure: figures latest_v3 7.pdf

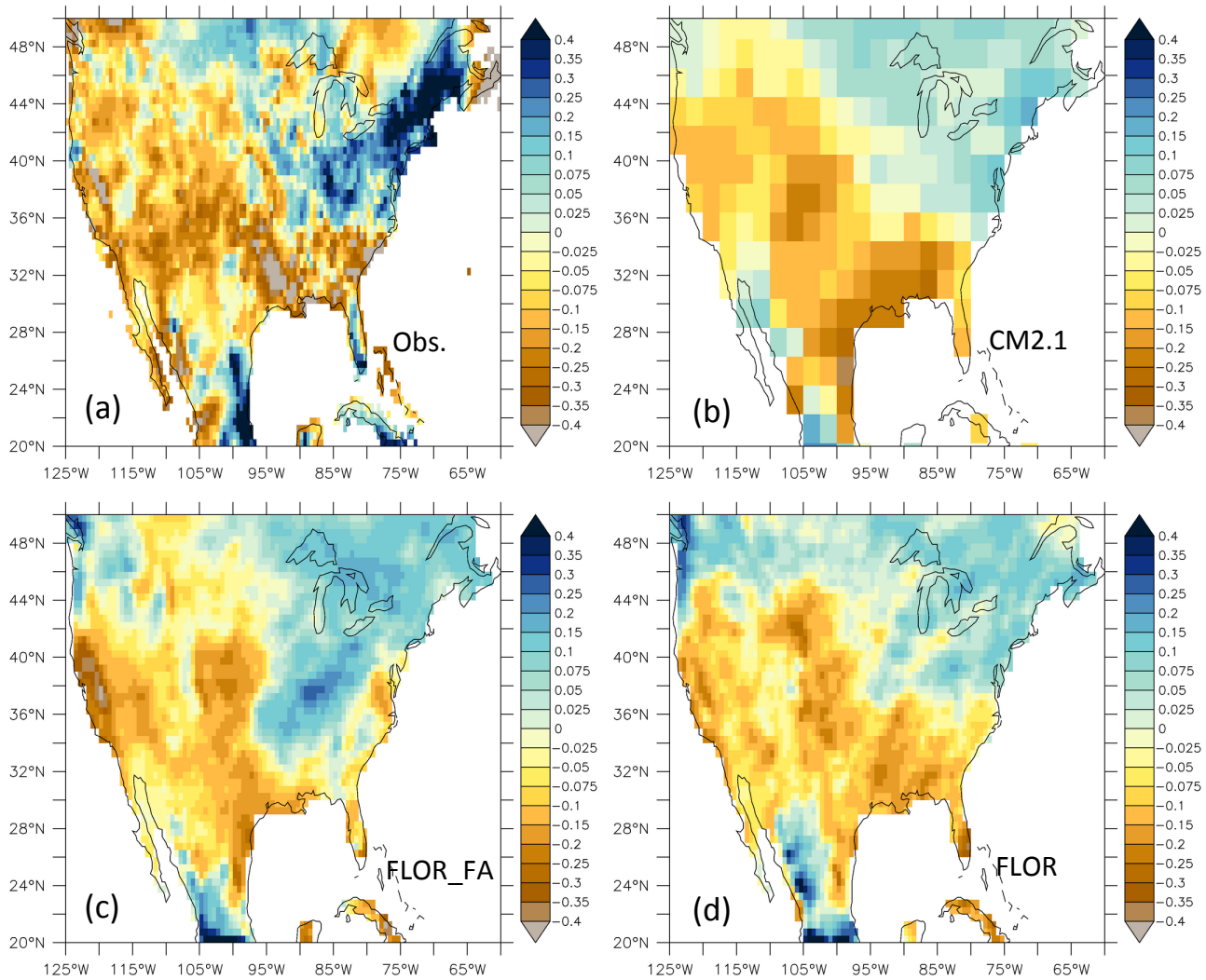

Figure 7 (a) Difference in observed annual mean precipitation for the period 2002-2012 minus 1979-2000. Observations are from the Climatic Research Unit of the University of East Anglia. Units are mm day^{-1}. (b) Same as (a) using model results from CM2.1 ALLFORC_STRESS, showing the combined effects of wind stress and radiative forcing changes. (c) Same as (b) using FLOR_FA. (d) Same as (b) using FLOR.

Rendered Figure 8

Click here to download Rendered Figure: figures latest_v3 8.pdf

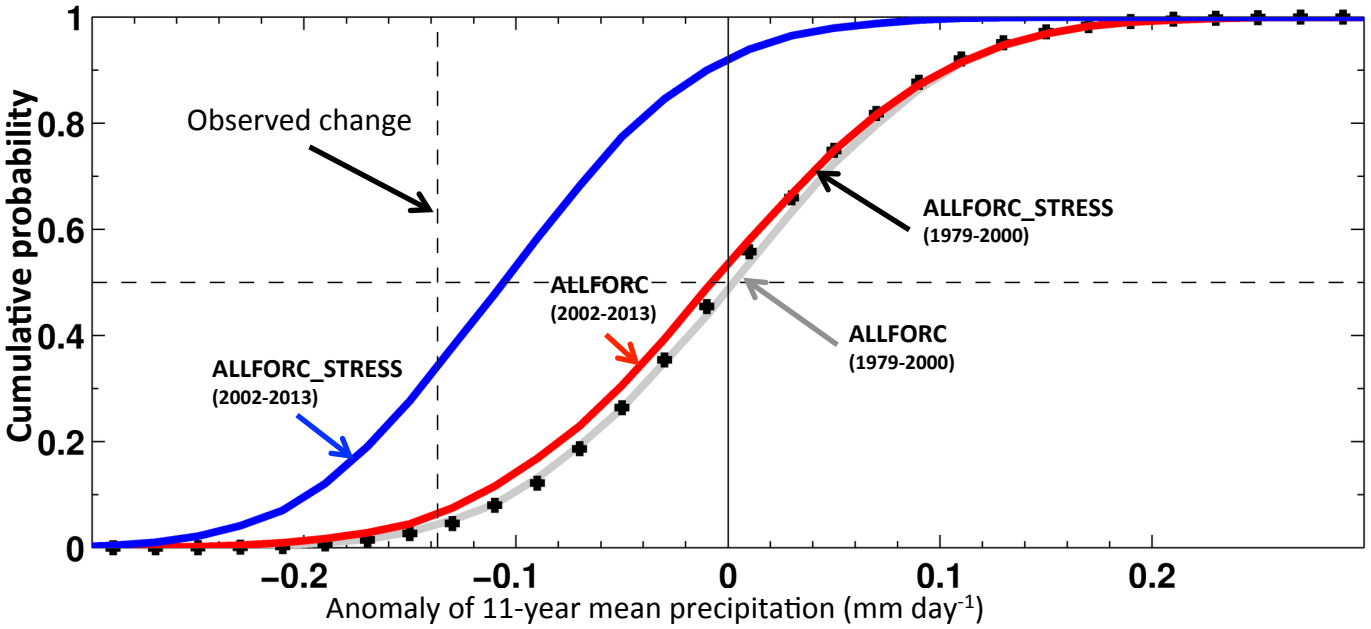

Figure 8 Cumulative probability distribution of 11-year mean precipitation anomalies (mm day^{-1}) averaged over 130^{0}W-95^{0}W, 30^{0}N-42^{0}N, land only. Grey curve (black crosses) indicates results using model values from the period 1979-2000 from experiment ALLFORC (ALLFORC_STRESS) using all three models (CM2.1, FLOR, FLOR_FA). Red (blue) curve denotes values from ALLFORC (ALLFORC_STRESS) over the period 2002-2012. The distributions are generated by resampling all ensemble members from each model (CM2.1, FLOR, FLOR_FA) for the experiment and period indicated. For example, for the grey curve we use output from all ten ensemble members of experiment ALLFORC, as well as five ensemble members each from FLOR and FLOR_FA, over the period 1979-2000 (440 total points, based on 22 years and 10 ensemble members from CM2.1, and 5 ensemble members for 22 years for FLOR and FLOR_FA respectively). We randomly pick 11 different values from among this pool of 440 values, and then average those to form an 11-year mean, and then subtract from that the ensemble mean value over the period 1979-2000. We repeat this process 10,000 times to form a distribution of 11-year mean anomalies, and plot that as a cumulative probability distribution function. We repeat this process using years 1979-2000 from ALLFORC_STRESS, years 2002-2012 from ALLFORC, and years 2002-2012 from ALLFORC_STRESS.

Rendered Figure 9
Click here to download Rendered Figure: figures latest_v3 9.pdf

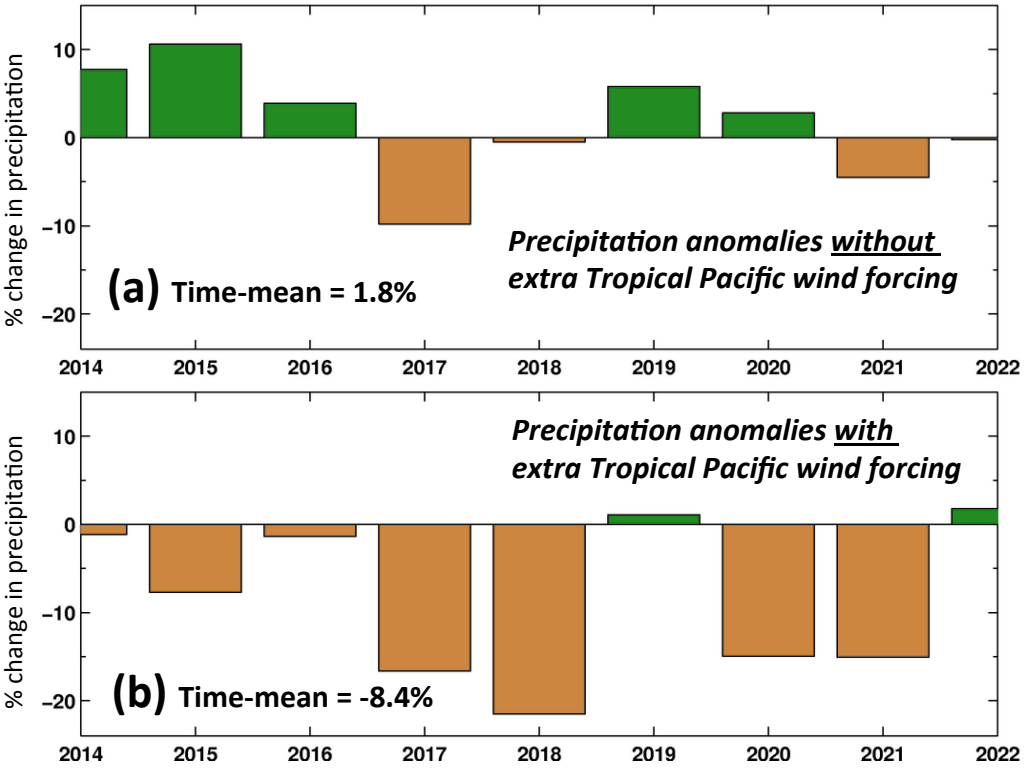

Figure 9 Time series of simulated percentage change in annual mean precipitation relative to the 1979-2000 time-mean, spatially averaged over 130°W-90°W, 30°N-42°N (land only). The simulations used the CM2.1 model, were 10-member ensembles, and started from identical initial conditions at the end of experiment ALLFORC_STRESS. (a) Precipitation change with no wind forcing anomaly in tropical Pacific. (b) Precipitation change when observed wind stress anomalies over the period 2005-2013 are applied to the model over the period 2014-2022.

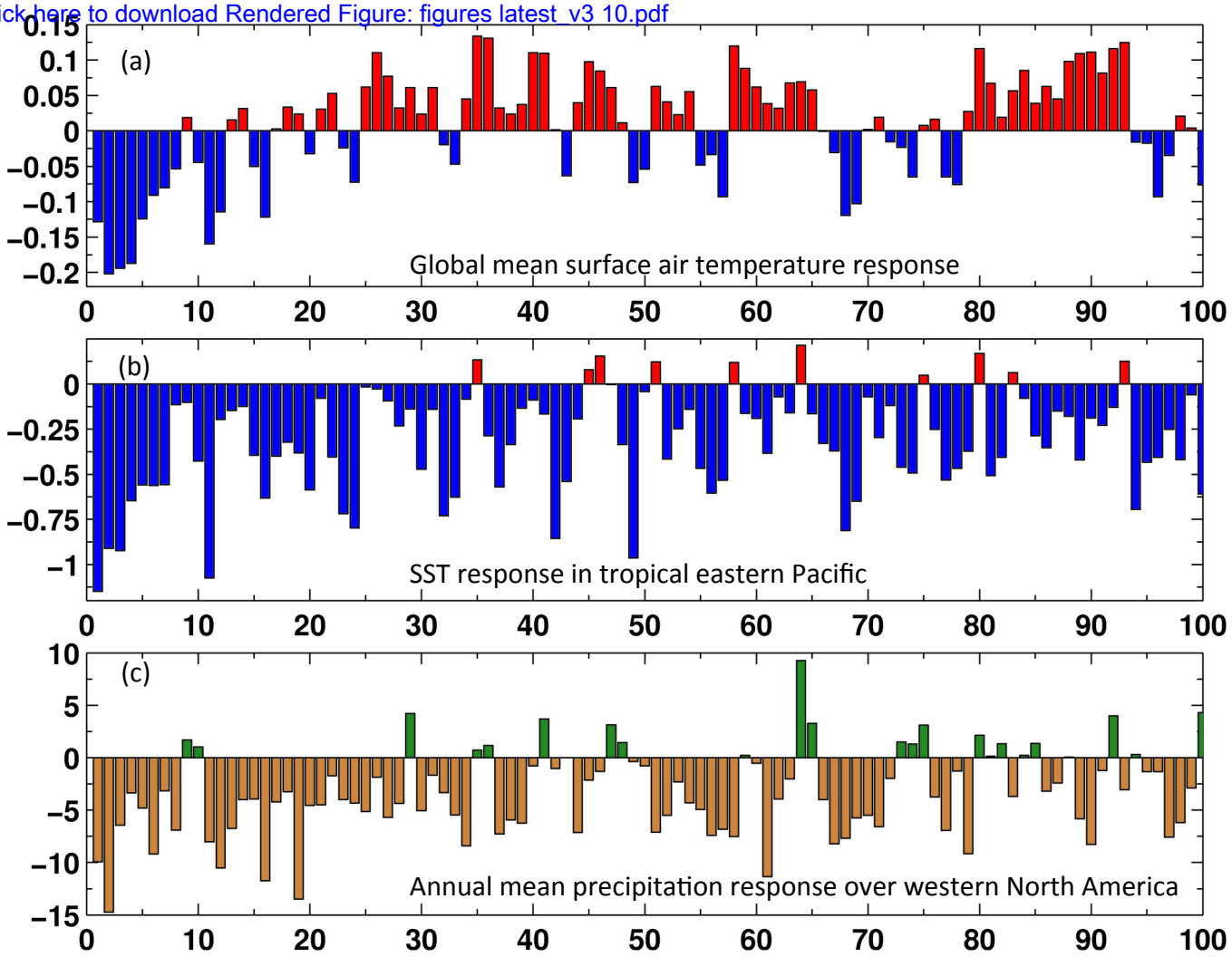

Figure 10 Response of temperature and precipitation to sustained addition of anomalous easterly wind stress in the tropical Pacific. (a) Time series of global mean surface air temperature response, calculated as global mean temperature in CONTROL_STRESS minus CONTROL. (b) Same as (a), but for SST averaged over a portion of the tropical eastern Pacific (170°W-100°W, 10°S-10°N). (c) Same as (a), but for annual mean rainfall averaged over 130°W-90°W, 30°N-42°N, land areas only, expressed as percentage change from long-term mean.

Rendered Figure 11
Click here to download Rendered Figure: figures latest_v3 11.pdf

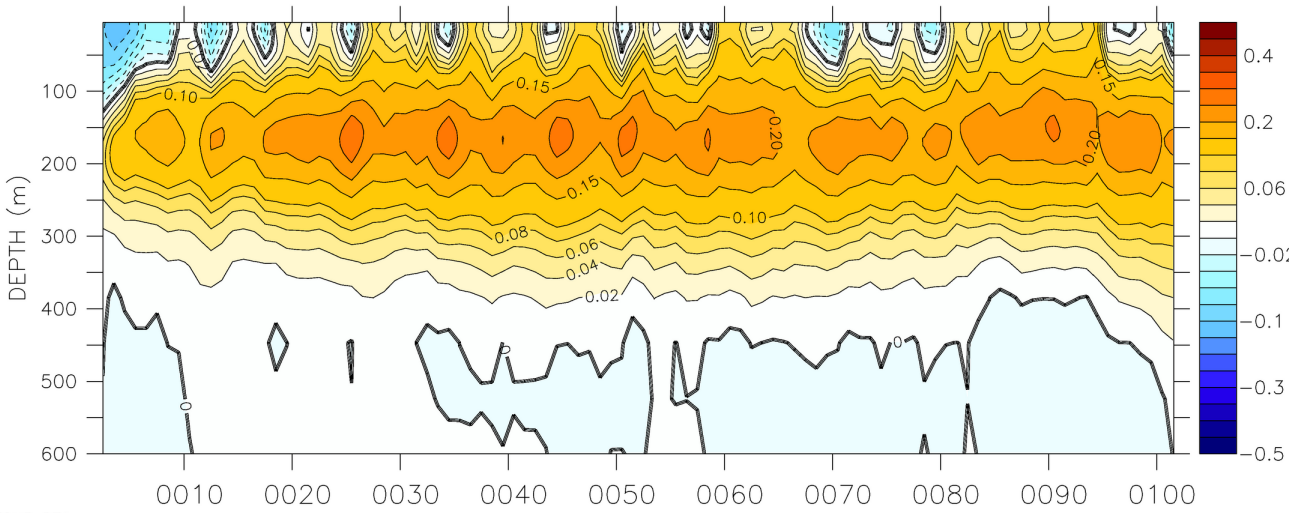

Figure 11 Response of global mean ocean temperature to sustained addition of anomalous easterly wind stress in the tropical Pacific, calculated as experiment CONTROL_STRESS - CONTROL. Positive values indicate a warming of the ocean in response to the anomalous easterlies.